

Discrepancies in Southern Hemisphere Mid-latitude Atmospheric Variability of the NCEP-NCAR and ECMWF Reanalyses

ALESSANDRO DELL' AQUILA⁽¹⁾, PAOLO M. RUTI⁽¹⁾, SANDRO CALMANTI⁽¹⁾ AND VALERIO LUCARINI⁽²⁾

¹*Progetto Speciale Clima Globale, Ente Nazionale per le Nuove Tecnologie, l'Energia e l'Ambiente, Roma, Italy*

²*Dipartimento di Matematica ed Informatica, Università di Camerino, Camerino (MC), Italy*

Corresponding author:

Dr. Alessandro Dell'Aquila

ENEA, C.R. Casaccia,

Via Anguillarese 301, 00060 S. Maria di Galeria, Rome, Italy

E-mail: alessandro.dellaquila@casaccia.enea.it

Phone:+39-06-30484072

Fax:+39-06-30484264

Abstract

In this paper we compare the representation of the southern hemisphere midlatitude winter variability in the NCEP-NCAR and ECMWF reanalyses. We use the classical Hayashi spectral technique, recently applied to compare the description of the atmospheric variability in the northern hemisphere on different spectral sub-domains as provided by the two reanalyses. We find relevant discrepancies in the description of the variability at different spatial and temporal scales. ERA40 is generally characterised by a larger variance, especially in the high frequency spectral region. In the southern hemisphere, also in the satellite period, the assimilated data are relatively scarce, predominately over the oceans, and they provide a weaker constraint to the model dynamics. In the pre-satellite period the discrepancies between the two reanalyses are large and randomly distributed while after the 1979 the discrepancies are smaller but systematic. Moreover, a sudden jump in the VTPR period (1973-1978) is observed, mostly in the ERA40 reanalysis. Our result suggest some caveats in the utilization of reanalysis data for the description of the midlatitude southern hemisphere variability.

1. Introduction

Reanalysis products are designed to obtain global, homogeneous and self-consistent datasets of the atmospheric variables on decadal periods to study atmospheric dynamics, to validate and initialise GCM and to detect eventual global climate changes. Recently, the National Center for Environmental Prediction (NCEP), in collaboration with the National Center for Atmospheric Research (NCAR) (Kistler et al., 2001), and the European Center for Mid-Range Weather Forecast (ECMWF) (Simmons and Gibson, 2000) have released re-analysed datasets for the time frames 1948-2004 and 1957-2002, respectively. We henceforth refer to such reanalyses with the names of NCEP and ERA40.

In a recent paper (Dell'Aquila et al, 2005; hereafter D05), the authors have compared the midlatitude variability in the NCEP and ERA40 reanalyses at different time and spatial scale for the overlapping period 1957-2002. D05 have used a standard space-time transformation (the Hayashi technique), to discriminate the variance associated with eastward/westward propagating and standing waves. Integral measures of the variance have been introduced in order to characterize the portion of the spectrum associated with the total, standing, eastward and westward propagating component, and their temporal evolution. This technique provides some synthetic and global information about the mid latitude tropospheric waves, by furnishing a spectral measure of their variance.

By using these spectral quantities, D05 have found some discrepancies in the description of variability in the two reanalyses taken into account. In particular, the differences are systematic in the pre-satellite period and spatially distributed principally over the oceanic basins. After the satellite introduction the accordance becomes closer, even if a systematic difference remains over the Pacific basin where ERA40 has a variance greater than one described in NCEP. In the pre-satellite period and over the oceans, the assimilated data are scarcer and they provide a weaker constraint to the model dynamics. Therefore, the resulting discrepancies in the reanalysis products may be mainly attributed to differences in the models' behaviour.

The results presented in D05 form the basis for the comparison of the mid latitude Southern Hemisphere (hereafter SH) winter variability in the NCEP and ERA40 reanalyses which we report in this paper. It is of paramount importance to assess the consistency of these reanalyses in representing the atmospheric variability in the SH, mainly where data are scarcer and they provide a weak constraint on the model behaviour. Recent works (see among others, Sterl 2004) have highlighted some relevant differences in the southern hemisphere between the two reanalyses by

analysing monthly averaged variables. Our aim is to detail the comparison between different reanalyzed products, applying the spectral technique used in D05, and focusing on the SH mid-latitude variability over different spatial and temporal scales.

A spectral approach to study the SH mid-latitude variability was considered by several authors during 80s (Mechoso and Hartmann, 1982; Fraedrich and Kietzig, 1983; Hansen et al., 1989). The spectral variance reveals a predominance of short and long eastward travelling waves, while differences respect to the Northern Hemisphere are detected for ultra-long period fluctuations. The SH mid-latitude variability has some peculiar features related to the geographical distribution of ocean and land, and it exhibits a greater zonal symmetry than in the Northern Hemisphere. During JJA, high frequency activity extends over a broader range of latitude in relation with the polar jet stream, while the low frequency variability is mainly associated with the polar jet stream (Trenberth, 1991). The high and low frequency components can not be treated separately, but they strongly interact each other. Cuff and Cai (1995) have shown the existence of a symbiotic relationship between the high and low frequency transients in the SH. On the low frequency time-scale (10-50 days), the preferred patterns of midlatitude variance are mainly eastward propagating trains, characterised by zonal wavenumber 4 and 5, the later becoming more prominent in the austral summer (Kidson, 99). The spatial confinement of the low frequency variance on the pacific ocean, observed also by Kidson, 99) can be explained by a large ensemble of high frequency passages, forced by tropical convection (Redwick and rewell, 1999). This flow feature has been defined in the past as a SH blocking. (Tibaldi et al, 1994).

Moreover, the most part of the detected trends related to an eventual climate change are recognized in the southern hemisphere (see, as example, Santer et al., 2003 JGR). So, our analysis could have a relevant role in the framework of atmospheric dynamics, in the climate description and also in studies of climate change.

The paper is organized as follows. In Section 2 we review the main differences between the reanalysis systems and describe the data used . In Section 3 we show the results of Hayashi spectral analysis for the two datasets and discuss the emerging differences. In Section 4 we compare the spatial distribution of the variability for the two datasets before and after the introduction of satellites observations. In Section 5 we summarize the results obtained and present our conclusions and outlook for future studies. Finally, we report in Appendix a full account of the spectral technique and the notation adopted.

2. Data

We use the freely available southern hemisphere 500hPa daily geopotential height fields provided by the NCEP and ERA40 datasets. We consider the datasets for the overlapping time frame ranging from September 1st 1957 to August 31st 2002. Both reanalyses are publicly released with spatial resolution of $2.5^\circ \times 2.5^\circ$, with a resulting horizontal grid of 144 x 73 points. We select the June-July-August (JJA) data relative to the latitudinal belt 30°S - 75°S (similarly to what done in D05 for the NH), where the bulk of the baroclinic and of the low frequency planetary waves activity is observed (Simmonds and Keay 2000; Trenberth 1991).

The principal inhomogeneity in the assimilated data is the introduction of satellite observations (systematically used since 1979) which has dramatically improved the amount of data principally in the southern hemisphere over the last three decades (Sturaro, 2003). The first source of satellite data for reanalysis is the Vertical Temperature and Pressure Radiometer (VTPR), available from 1973 to 1978. treated in very different ways in the two assimilation systems. The inhomogeneity related to VTPR, already pointed out in D05, could be more relevant in the southern hemisphere for the lack of other data sources. Moreover, in the Southern region there are well known processing errors in the reanalyses assimilation, as the misplacing of PAOBS data in NCEP (Kistler et al 2001) for the period 1979-1992. Studies at the Climate Prediction Center into the sensitivity of the NCEP reanalysis to the misplaced PAOBS indicate that the largest differences for wintertime synoptic-scale features are seen poleward of 40°S over the oceans in the winter months, and decrease rapidly with height. Analyses of synoptic-scale features south of 40°S in 1979-1992 could be affected by the addition of an error that has a magnitude comparable to the basic uncertainty of the analyses. (Kistler et al 2001, Simmonds and Keay 2000)

In order to provide a rough estimate of this bug, we have also taken into account the NCEP-DOE AMIP II reanalysis (hereafter NCEP2) that fixes this mistake and several previous processing errors present in NCEP (see Kanamitsu 2002, where a detailed description of NCEP2 is reported).

NCEP2 has been released for the time frames 1979-2002. NCEP2 should not be considered as a different reanalysis, but should be regarded as an updated and human error-fixed version of NCEP. The physical parameterisations are the same used in NCEP, with the same spatial and temporal resolution, and the satellite data are treated in the same way.

For a more detailed description of the reanalysis systems we refer to Sec. 2a of D05.

3. Hayashi spectra

3a. Climatological average

The spectra express the power density of the wave field with respect to frequency and zonal wavenumber, and its decomposition into standing and propagating components. Fig. 1a shows $\overline{H}_T(k_j, \omega_m)$, the total power spectrum; Fig. 1b shows $\overline{H}_S(k_j, \omega_m)$, the power spectrum related to standing waves; Fig. 1c shows $\overline{H}_E(k_j, \omega_m)$, the power spectrum related to eastward propagating waves; Fig. 1d shows $\overline{H}_W(k_j, \omega_m)$, the spectrum of the westward propagating waves. The overbar indicates the operation of averaging over 39 winters. Throughout the paper, $k_j = 2\pi j$ is the zonal wavenumber, $\omega_m = 2\pi m/\tau$ is the frequency of the wave with $\tau = 90d$ defined as length of each winter, and the indexes T , S , E , and W indicate total, standing and eastward/westward propagating components, respectively. As customary in literature, the Hayashi spectra have been plotted after multiplying the power spectra by $j \cdot m$, in order to compensate for the non-constant density of points in a log-log plot (see Appendix A for notation and more details).

We underline that the Hayashi spectra computed using this definition result to be expressed in units of m^2 as done by Blackmon [1976] and Speranza [1983] and must be multiplied times a factor $1/8 \cdot 86400s$ to be comparable with what shown in D05 (where the spectra were expressed in m^2 / s).

The lobes of westward propagating components (reported in Fig. 1b-d) are less intense and bounded on the planetary scale (zonal wavenumbers 2-3, periods longer than 20 days), as expected in a region with a large scale topography present but small.

The variability is essentially explained by the eastward propagating component, that is more active than the corresponding one in the northern hemisphere (see Fig. 1c in D05) and also characterises the planetary spatial and long time scale ($k=4$ and period around 15 days), as illustrated in Fig. 1c. Note in particular that the amplitude of the variability associated to $k=4$ is double with respect to corresponding one in the NH. This component mostly coincides with the total variance shown in Fig. 1a and could be related with the blocking episodes (Renwick and Revell, 1999). The standing variance is essentially comparable with that observed in the Northern hemisphere. From this feature we can also hypothesise that in the large-scale circulation the topography is more relevant for the travelling waves than for the standing ones. These results are in good agreement with the past

analyses performed along the same lines but using shorter datasets (Fraedrich and Kietzig, 1983; Hansen et al.1989).

Following D05 we analyse the difference between the description of the climatological variance of the two reanalyses obtained by using the Hayashi technique. In Fig. 2 we report the difference in the climatological spectra of eastward propagating component between ERA40 and NCEP. As clearly shown in this Figure, ERA40 dramatically overestimate the variance relative to eastward propagating component of the wavy field. The observed discrepancy corresponds to more of 25% of the signal. The other components do not show any relevant difference. The discrepancies are most evident for zonal wave number $k=5$ and for a period of about 7 days, in the spectral region of baroclinic disturbances. It is quite impressive to observe the amount of this difference that points out that the Climatologies of the winter atmospheric variability in the southern hemisphere of the two datasets are almost different. Let us also note that these differences in the southern hemisphere variability are quite greater than the corresponding in the northern one. Finally, we compare with the climatological averages of ERA40 also those obtained by NCEP2 for the overlapping period (1979-2002) and we obtain almost the same result (here not shown).

3b. Interannual variability

Following D05, we inspect the temporal behaviour of the previously observed discrepancies by using introduce the following integral quantities $E_j^n(\Omega)$ that represent the portion of variance associated to specific spectral subdomains Ω . In Appendix B we report the definition of the integral quantities and a review of this methodology. We underline that the quantities $E_j^n(\Omega)$ considered in this paper are conveniently expressed in unit of m^2 and must be multiplied by a conversion factor to be comparable with the values presented in D05.

In the first two columns of Table 1 we report the time average $\bar{E}_j(\Omega)$ for the two reanalyses, computed over the whole wavenumber and frequency domain for the overlapping period 1957-2002. As in D05, we estimate the standard error of the time-averaged value with the interannual

variability of the signal: $\Delta_{E_j(\Omega)} = \frac{\sigma_{E_j(\Omega)}}{\sqrt{N}}$, where N is the number of winters considered in the

averaging process, since winters are statistically independent from each other. Most of the variance is due to the eastward propagating component, as can be inferred also from Fig. 1. The time-average of the ERA40 signal is considerably larger and the discrepancies between the averaged values for

NCEP and ERA40 largely exceed the error bar related to the standard error $\Delta_{E_j(\Omega)}$, specially for the eastward propagating waves.

Inspection of the differences in $E_j^n(\Omega)$ for the total, standing and eastward/westward propagating components (Fig. 3), reveals a bias of ERA40 towards larger $E_j^n(\Omega)$ in the period 1958-1972, with a principal contribution from the eastward propagating component.. However, in this period the signal-to-noise ratio for the discrepancies between the two reanalyses is small. Moreover, in the standing and westward propagating component there is no clear shift. There is an sudden jump in 1973 when the propagating eastward variance observed in ERA40 abruptly decreases with respect to NCEP. Another abrupt jump can be observed in 1978. Afterwards, ERA40 exhibits a systematic larger variance. This result does not change if we consider a different latitudinal belt (30S-50S or 50S-70S, here not shown).

The abrupt change in the description of the variability correspond to the use of VTPR data (as largely discussed in D05). This result suggests that the different use of satellite data (NCEP system assimilates retrieved profiles of temperature and humidity, ERA40 assimilates directly satellite radiance) corresponds to a very different capability in describing atmospheric variability, principally the travelling disturbances. This effect is particularly evident in the southern hemisphere where a weaker constraint on the models is provided by the sparse land-based vertical soundings available.

In order to compare data which are derived homogeneously, we have decided to skip the VTPR period 1973-1978 when we observe a very different feature with respect the previous and the following period. We exhibit in Table 1 averaged values $\bar{E}_j(\Omega)$ for the pre-satellite period (1958-1972) and for 1979-2002. For both periods the ERA40 mean values are clearly larger than for NCEP with differences significantly greater than the corresponding standard error $\Delta_{E_j(\Omega)}$. We can also note an abrupt change in $\bar{E}_{T,E}(\Omega)$ between the first and the second period in ERA40, as already pointed out by Bengtsson et al 2003 who analysed different climatological variables. In NCEP the time averaged values seem to be more homogeneous. Nevertheless, a trend in the measure of variance is also recognizable by an inspection of time averages above the two periods, as also noted by Renwick and Revell (1999)

To analyse the effects of the bugs corrected in NCEP on the description of the midlatitude variability, we compare also the differences in $E_j^n(\Omega)$ for NCEP and NCEP2 for the overlapping period 1979-2002. As shown in Fig. 4, the discrepancies between the two releases of the NCEP-NCAR reanalysis are one order magnitude smaller than the ones found between NCEP and ERA40.

However, these differences are comparable with the ones relative to the northern hemisphere between NCEP and ERA40 (D05) and they are not negligible. In particular, the discrepancies are more pronounced in the first years, when NCEP data are affected by the well known PAOBS bugs and every component $E_j^n(\Omega)$ equally contribute to the total difference. So, we have estimated that the known bugs in the NCEP reanalysis have a minor role in the observed discrepancy between the two reanalyses in exam.

Following D05, in Table 2 we propose the clear-cut division of different spectral sub-domains Ω into four categories, on the basis of the results reported in Fig. 1a-d. This partition can help identifying discrepancies in the capability of the two reanalyses in describing phenomena occurring on a given spatial and temporal scale and pertaining to different physical processes. As well as in the Northern hemisphere, also in the austral winter most of the variance has to be attributed to the Low Frequency- Low Wavenumber (LFLW) and High Frequency High Wavenumber (HFHW) waves (values not shown). However, the division is slightly different by the one adopted for the northern hemisphere for the dissimilar spectral properties of the ultra long and synoptic waves in the southern region.

In Fig. 5a-b we plot the time series of the difference between the integrals $E_j^n(\Omega)$ computed over the subdomains LFLW and HFHW, for the two reanalyses. The behaviour exhibited in Fig. 3 is substantially confirmed. For the discrepancies in LFLW (Fig. 5a) the signal-to-noise ratio is small in the pre-satellite period. Let us also note that ERA40 has, on average, a lesser standing variance than NCEP. Then, after a sudden jump in the VTPR period, the differences become systematic. In the HFHW spectral subdomain (Fig. 5b) the discrepancies seem to be noisy in the earlier period but ERA40 has systematically more variance than NCEP. After the 1979 the noise-to-signal ratio becomes greater and the differences are almost constant.

4. Spatial distribution of variability before 1973 and after 1979

In Section 3 we have examined the discrepancies emerging from a synthetic description of the activity of planetary and synoptic waves. In Fig. 3, a sudden shift in the systematic bias was observed in 1973 corresponding to the first introduction of VTPR data. A second shift is apparent in the late 1970s when standard satellite observations began to be regularly employed. After the introduction of the satellite data the discrepancy is systematic and ERA40 shows a larger variance. We now proceed by analysing the spatial distribution of the differences between NCEP and ERA40.

In Fig. 5a-d we map the low frequency (LF) variability of NCEP for the periods 1958-72 (Fig. 6a) and 1979-2002 (Fig. 6b), and the corresponding differences with the same data for the ERA40 reanalysis (Fig. 6c-6d, respectively). The LF atmospheric variability is obtained by discarding the frequencies $\omega > 2\pi/11 \text{ day}^{-1}$ (see also Table 2) in a Fourier transform of the 500hPa geopotential height. The two maps of the NCEP variance show that the LF atmospheric variability appears more symmetric than the corresponding northern one. However, two maxima over the Pacific and Indian basins are well defined. Over these regions the major discrepancies between the two reanalyses occur. In particular, before the 1973 (Fig. 6a) an East-West dipole structure is evident over the Pacific region. This suggests a different location of the LF variability maximum, as reproduced in NCEP and ERA40. A similar pattern, but with axes North-South oriented, is present also over the Atlantic basin. In the Indian sector ERA40 overestimate the LF variance with respect to NCEP. In the south of Australia the differences are almost comparable with the signal itself. After 1979, ERA40 has systematically more variance than NCEP, especially over the south Pacific region. The spatial pattern of the high frequency (HF) variability ($10 \text{ day}^{-1} \leq \omega \leq 2\pi/2 \text{ day}^{-1}$, as in Table 2) is reported in Fig. 7. In Fig. 7a-b is reported the well known pattern of the southern storm track characterised by a greater zonal symmetry than the northern one and that remains near 50°S mainly over the Indian Ocean. (Trenberth 1991). As reported in Fig. 7c-d, in both periods, ERA40 has more HF variability on the entire southern mid-latitude band; the relative differences are of the order of 30%, with peaks of about 40% over the Indian Ocean, in the southern hemisphere storm track region. However, unlikely observed in Fig. 6 for the LF, in the HF region the introduction of the satellite do not drastically modify the discrepancies observed in the two reanalyses

5. Discussion and conclusions

In this paper the NCEP and ERA40 reanalyses have been compared for the overlapping period 1957-2002. Differences in the description of the southern hemisphere winter variability have been quantitatively estimated by employing the space-time Fourier decomposition introduced by Hayashi (1971; 1979), recently re-discussed in D05.

We have found a systematic difference in the description of variability in the two reanalyses for the period 1957-72. On average, ERA40 is characterised by a variance larger than NCEP, mainly in the region of the eastward propagating long ($k=4$, period=15d) and synoptic waves ($k=5$; period=7d). Additionally, by using ad hoc integral measures, we have inspected the temporal behaviour of the discrepancies in describing the southern hemisphere variability in the two reanalyses. We have

found an abrupt jump in the differences in the period corresponding to the introduction of VTPR data (1973-1978) and a systematic bias in the satellite period. The differences revealed are about 30% of the signal. In particular we find a sudden jump in the ERA40 variability in the 70s (see also Bengtsson 2004)

Then, we focused on two main spectral sub-domains (HFHW and LFLW), as in D05, which are in a strong “symbiotic” relationship in the southern hemisphere (Cai and Mak, 1990) because a more effective forcing of mid-latitude LF variability by HF. In the LF region there are randomly discrepancies in the pre-satellite period, where, after 1979, the discrepancies are systematic. On the other hand, ERA40 is always characterised by a larger HF variance, focused on the southern storm track region. No better accordance with ERA40 has been found using NCEP2 data, where some known bugs present in NCEP have been fixed.

From these results some conclusion can be pointed out that in the pre-satellite a weaker constraint on the models is provided by the sparse land-based vertical soundings available not sufficient to constraint the models to a similar behaviour. However, even after the introduction of satellite data in the assimilation systems, the different treatment of these data leads to a different representation of variability as observed also in the Northern Hemisphere for the Pacific sector (D05, Branckovic and Molteni, 2004). However, in some southern regions only satellite data are available and they are not enough to constrain the models to a similar representation of the atmospheric variability.

Some caveat could be introduced regarding to what asserted by Kidson (1999) about the period 1970-73 when a different behaviour of LF variability is observed. During this period different data and different assimilation methods have been used in the assimilation systems. Thus, a caution should be used for direct comparison of atmospheric fields in different periods. Moreover, several recent work (among others, Santer et al 2003) revealed some decadal changes in monthly averages data from reanalyses in the southern hemisphere. These trends could be influenced by the major changes in the observing system which occurred in 70s (see also Bengtsson et al 2004).

The differences observed around the wave number 4 can be ascribed to SH blocking episodes (Renwick and Revell, 1999), and in turn related to a different representation of the tropical forcing in the two reanalyses. This discrepancy is probably due to a well known differences in the representation of tropical OLR, in particular over the deadline.

Finally, we wish to emphasize that this work (likely D05) could be considered also as a preliminary test for methodologies and diagnostics tools to be employed for the intercomparison of simulations such as those provided in the broader context of Program for Climate Model Diagnosis and Intercomparison (PCMDI), sponsored by the Intergovernmental Panel on Climate Change Assessment Report 4 (IPCC-AR4).

Acknowledgments.

We wish to thank A. Sutera and A. Speranza for useful suggestions.

APPENDIX A

The space-time spectral analysis, introduced by Hayashi (1971), provides information about the direction or speed at which the eddies move. This information may be obtained by firstly Fourier-analysing the spatial field, and then computing the time-power spectrum of each spatial Fourier component. The difficulty here lies in the fact that straightforward space-time decomposition will not distinguish between standing and travelling waves: a standing wave will give two spectral peaks corresponding to travelling waves moving eastward and westward at the same speed and with the same phase. The problem can only be circumvented by making assumptions regarding the nature of the wave. For instance, we may assume complete coherence between the eastward and westward components of standing waves and attribute the incoherent part of the spectrum to real travelling waves (Pratt 1976; Fraedrich and Bottger 1978; Hayashi 1979).

In this formulation, for each winter considered, we express the 500hPa geopotential height $Z(\lambda, t)$ in terms of the its zonal Fourier harmonic as:

$$(A2) \quad Z(\lambda, t) = Z_0(t) + \sum_{j=1}^{\infty} \{C_{k_j}(t) \cos(k_j \lambda) + S_{k_j}(t) \sin(k_j \lambda)\}$$

where the zonal wavenumber is expressed as $k_j = 2j\pi$.

The power spectrum $H_{E/W}(k_j, \omega_m)$ at a zonal wavenumber k_j and temporal frequency $\omega_m = 2\pi n/\tau$, where $\tau = 90d$ is the length of the winter, for the eastward and westward propagating waves is :

$$(A1a) \quad H_E(k_j, \omega_m) = \frac{1}{4} \{P_{\omega_m}(C_{k_j}) + P_{\omega_m}(S_{k_j})\} + \frac{1}{2} Q_{\omega_m}(C_{k_j}, S_{k_j})$$

$$(A1b) \quad H_W(k_j, \omega_m) = \frac{1}{4} \{P_{\omega_m}(C_{k_j}) + P_{\omega_m}(S_{k_j})\} - \frac{1}{2} Q_{\omega_m}(C_{k_j}, S_{k_j})$$

where P_{ω_m} and Q_{ω_m} are, respectively the power and the quadrature spectra of zonal Fourier harmonic of the 500hPa geopotential height $Z(\lambda, t)$.

The total variance spectrum $H_T(k_j, \omega_m)$ is given from the sum of the eastward and westward propagating components:

$$(A3) \quad H_T(k_j, \omega_m) = \frac{1}{2} \{ P_{\omega_m}(C_{k_j}) + P_{\omega_m}(S_{k_j}) \}$$

while the propagating variance $H_p(k, \omega)$ is given by the difference between the components (A1a) and (A1b):

$$(A4) \quad H_p(k_j, \omega_m) = |Q(k_j, \omega_m)|.$$

So, the standing variance spectrum $H_s(k, \omega)$ can be obtained by the difference:

$$(A5) \quad H_s(k_j, \omega_m) = H_T(k_j, \omega_m) - |Q(k_j, \omega_m)|.$$

We emphasize that for sake of simplicity of the notation, we have neglected the indication of the winter under investigation, denoted in the text by the superscript n . We emphasize that customarily, Hayashi spectra are generally represented by plotting the quantities $j \cdot m \cdot H_T(k_j, \omega_m)$, $j \cdot m \cdot H_S(k_j, \omega_m)$, $j \cdot m \cdot H_E(k_j, \omega_m)$, and $j \cdot m \cdot H_W(k_j, \omega_m)$, as reported in Fig. 1a-1d, in order for equal geometrical areas in the log-log plot to represent equal variance. With this definition, the Hayashi spectra presented in this paper are expressed in unit of m^2 and can be compared to those given in D05 after a multiplication by $1/8 * 86400s$

APPENDIX B

It is possible to go beyond the comparison of climatological averages of the Hayashi spectra by inspecting the temporal behaviour of the previously described discrepancies in specific spectral subdomains. We introduce the following integral quantities:

$$(B1) \quad E_t^n(\Omega) = \sum_{m=m_1, j=j_1}^{m=m_2, j=j_2} H_j^n(k_j, \omega_m), \quad \text{with } t=T, S, E, W;$$

where n indicates the winter; the integration extremes, $m_{1,2}$ and $j_{1,2}$, determine the spectral region of interest $\Omega = [\omega_{m_1}, \omega_{m_2}] \times [k_{j_1}, k_{j_2}]$. The quantity $E_t^n(\Omega)$ introduced in equation (B1) represents the portion of variance of the spectrum associated to a given subdomain Ω and to a given winter n and is expressed in unit of m^2 . The averaging process defined in equation (B1) overcomes the well-known instability of the Fourier analysis in describing small scale spectral features. The quantities $E_t^n(\Omega)$ considered in this paper are more convenient than the corresponding integral quantities presented in D05. The $E_t^n(\Omega)$ can be compared numerically to the integral quantities presented in D05 after multiplying them by a multiplicative constant $1/8 * 86400s$.

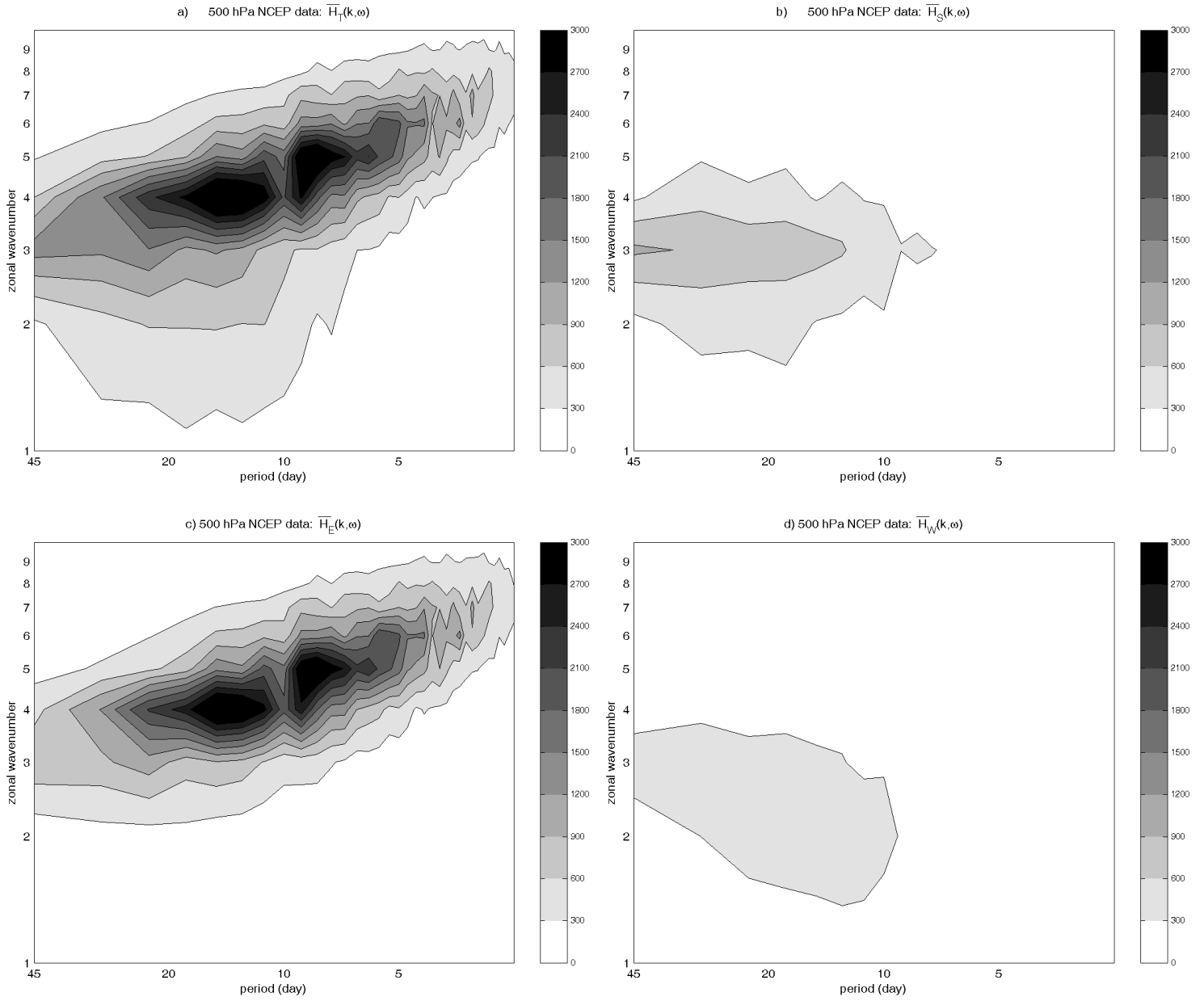


Figure 1: Climatological average over 45 winters of Hayashi spectra for 500 hPa geopotential height (relative to the latitudinal belt 30°S-75°S) from NCEP data: $\overline{H}_T(k_j, \omega_m)$ (a); $\overline{H}_S(k_j, \omega_m)$ (b); $\overline{H}_E(k, \omega)$ (c); $\overline{H}_W(k_j, \omega_m)$ (d). The Hayashi spectra have been obtained multiplying the spectra by $j*m$. The units are m^2

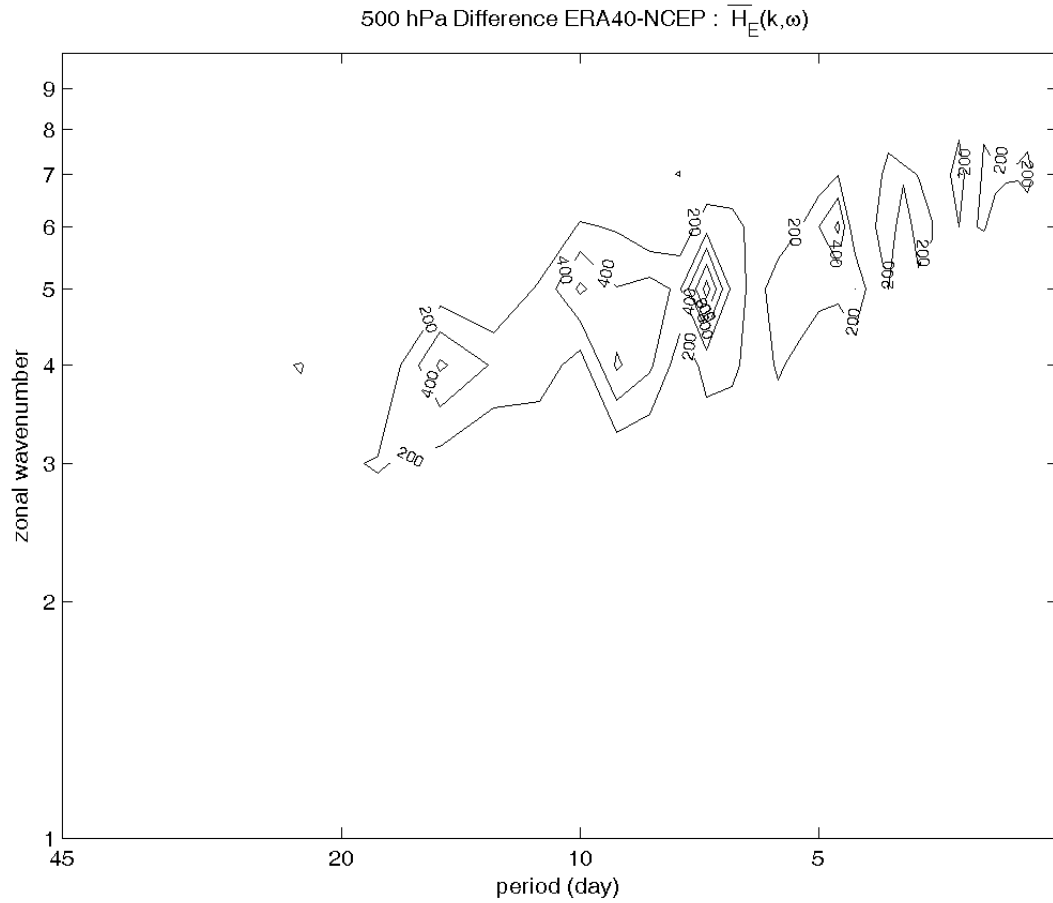


Figure 2: As in Fig.1c but for the difference between ERA40 and NCEP dataset Hayashi spectra. We do not plot the zero contours. In the standing and westward propagating component there are no significant differences and are not reported here.

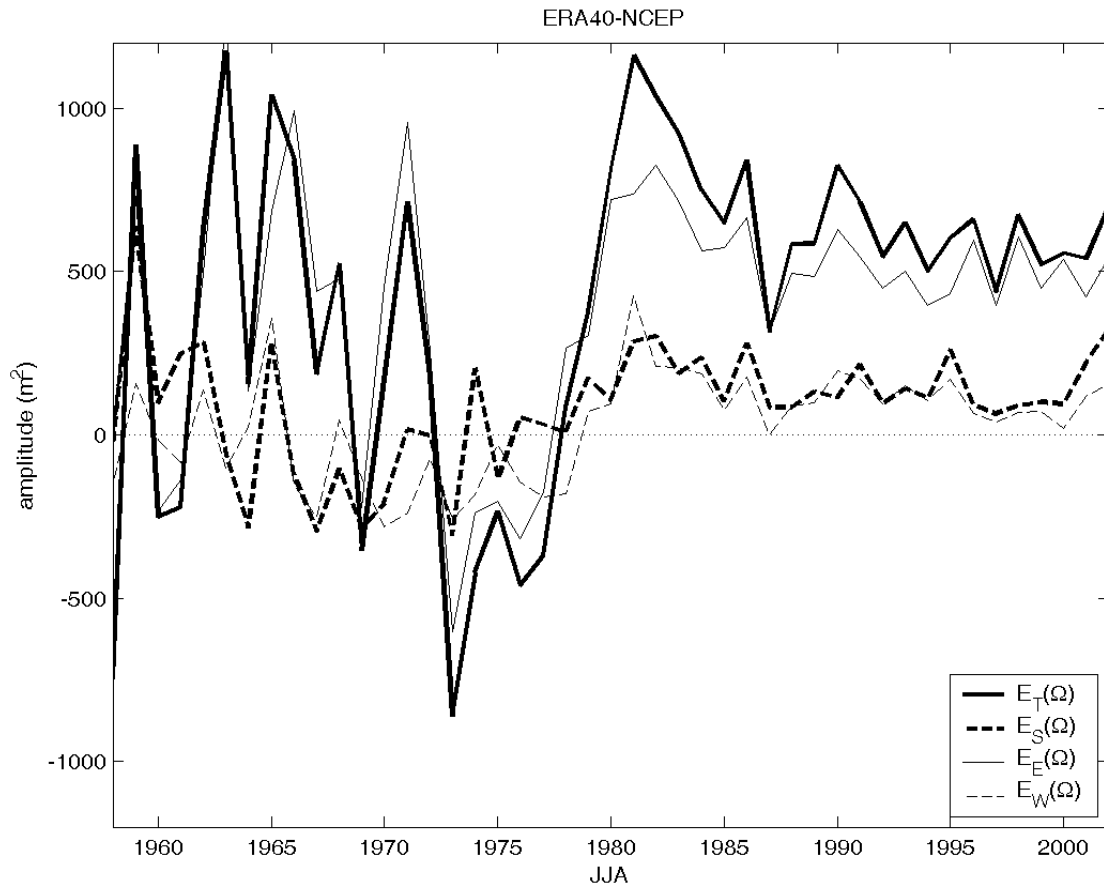


Figure 3: Time series of the differences of the quantity $E_j^n(\Omega)$ computed for the two reanalysis datasets, for: total variance (thick line), standing (dashed thick line), propagating eastward (thin line) and propagating westward (dashed thin line). Here, Ω corresponds to the whole wave number and frequency domain.

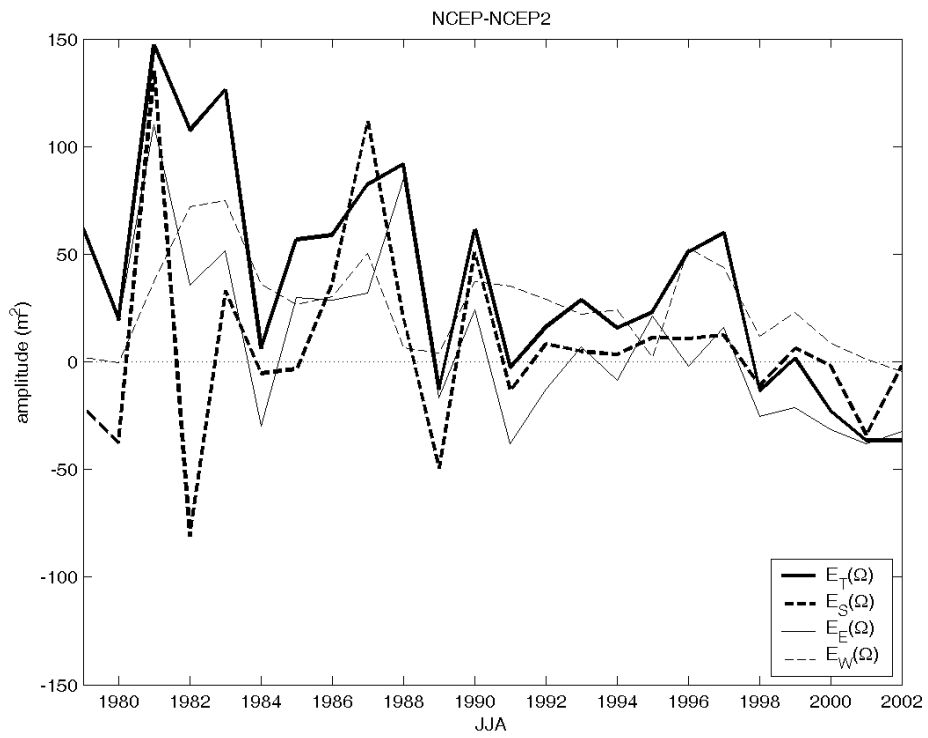


Figure 4: As in figure 3 for the differences between NCEP and NCEP2 .

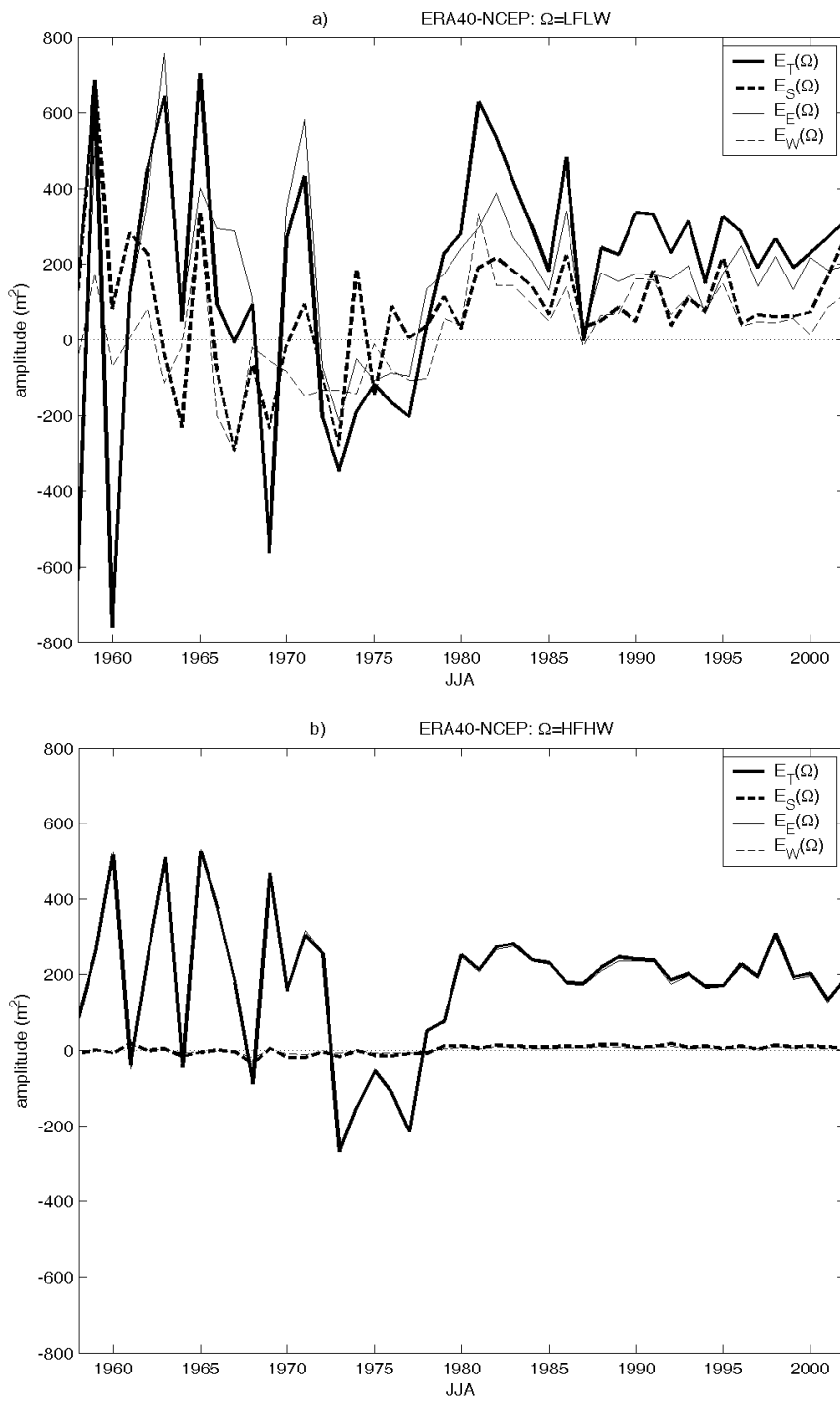
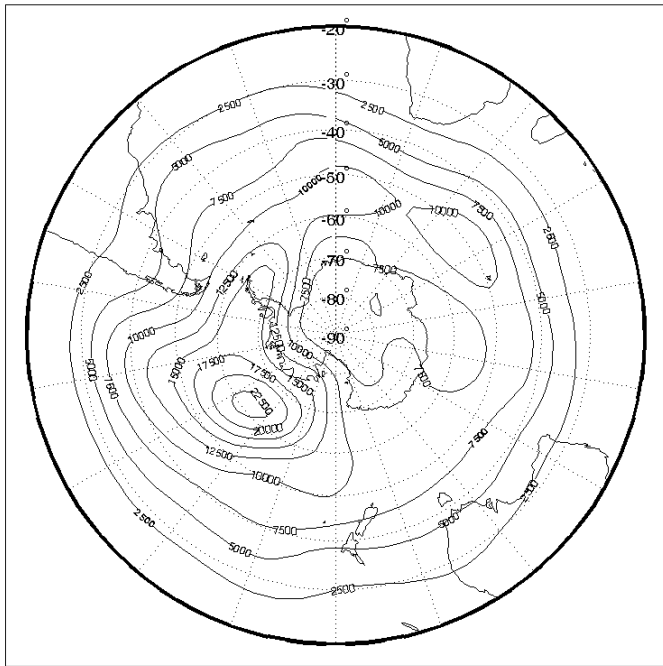
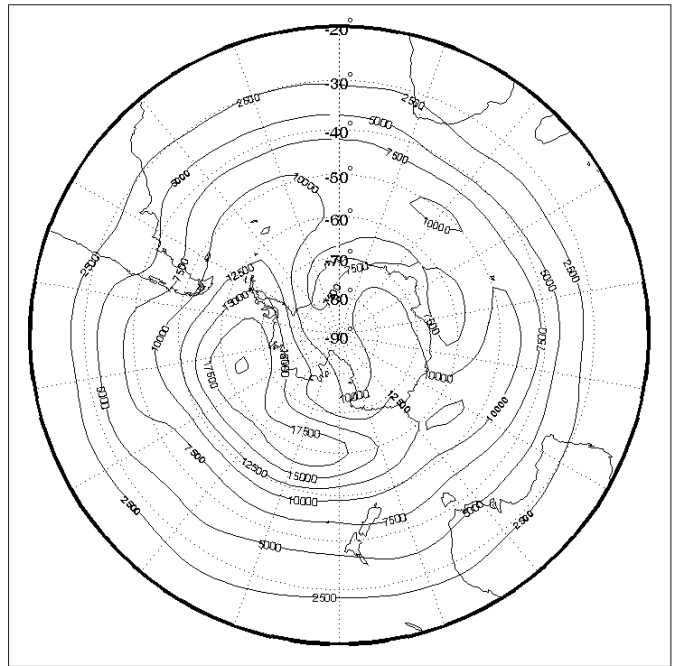


Figure 5: As in figure 3 for the categories *LFLW* (a), *HFHW* (b) described in Table 2.

a) 500 hPa Variance LF NCEP: 1958-1972



b) 500 hPa Variance LF NCEP: 1979-2002



c) 500 hPa Difference ERA40-NCEP Variance LF: 1958-1972



d) 500 hPa Difference ERA40-NCEP Variance LF: 1979-2002

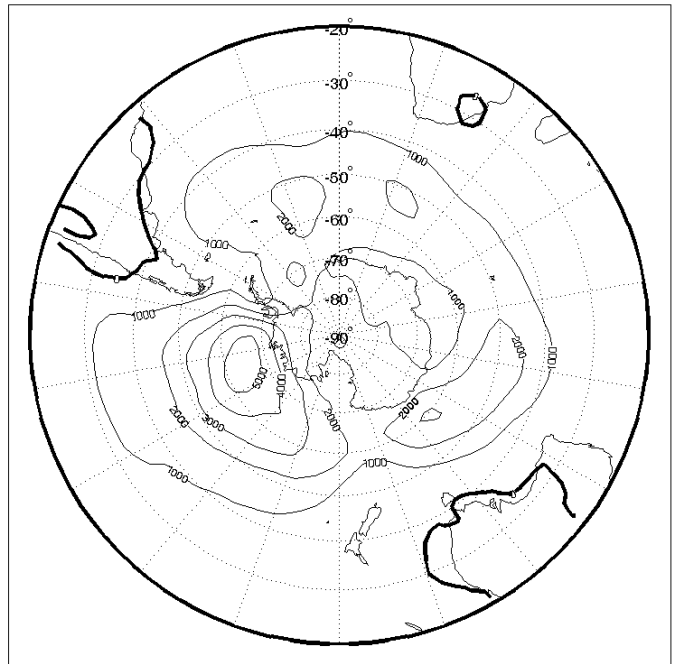
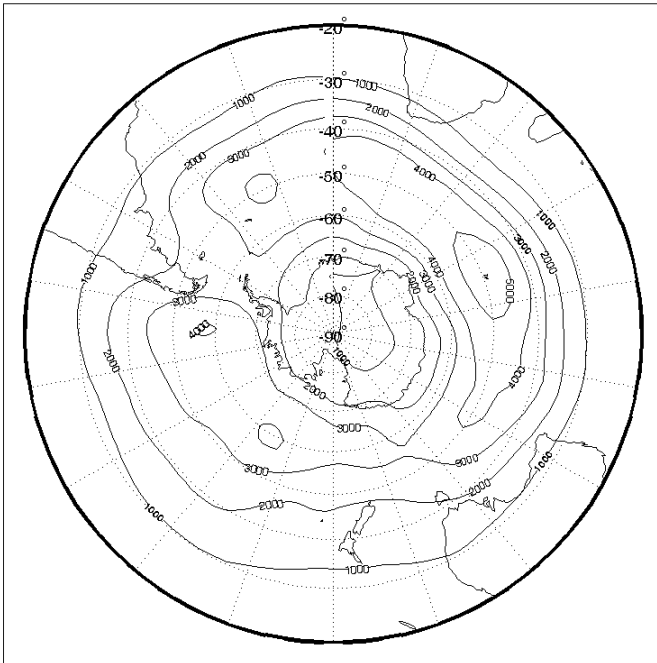
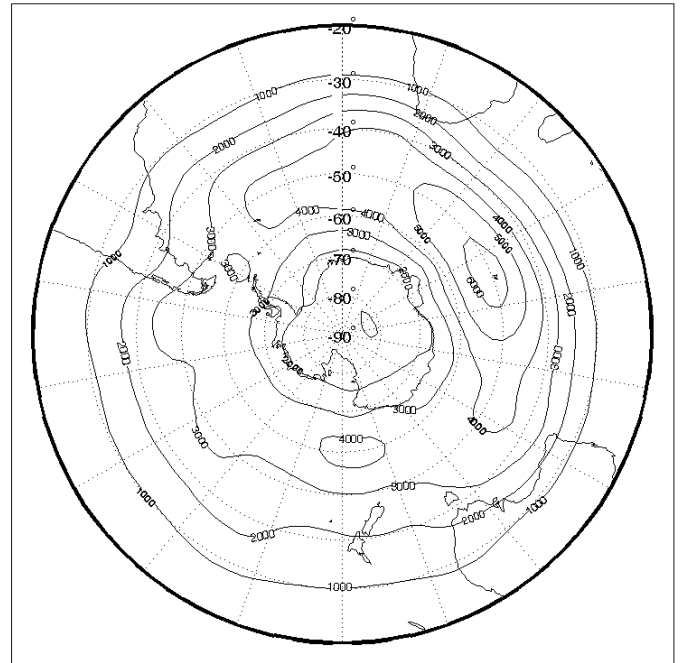


Figure 6: Low frequency variance of the 500 hPa geopotential height, JJA period: a) NCEP 1958-1972; b) NCEP 1979-2002; c) difference between ERA40 and NCEP, 1958-72; d) as c) for 1979-2002. Units are m^2 and contour interval is 2500 m^2 for a) and b) and 1000 m^2 for c) and d). Dashed lines pertain to negative values. Thick line corresponds to zero difference.

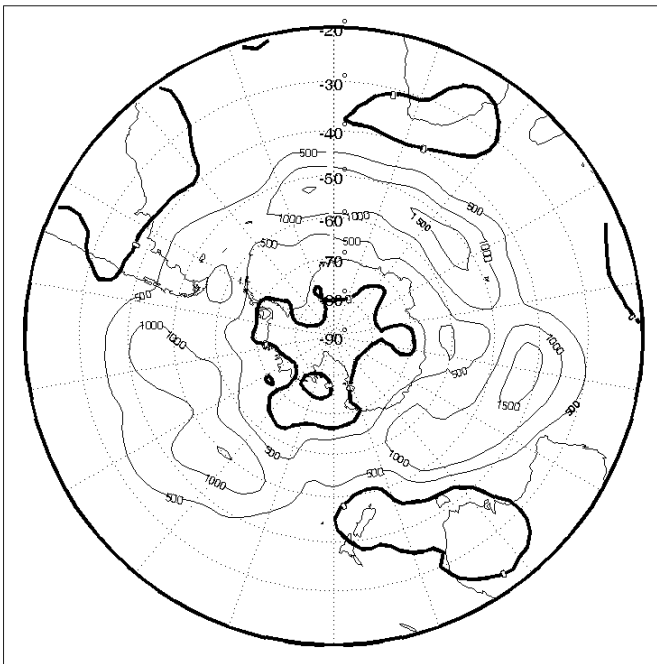
a) 500 hPa Variance HF NCEP: 1958-1972



b) 500 hPa Variance HF NCEP: 1979-2002



c) 500 hPa Difference ERA40-NCEP Variance HF: 1958-1972



d) 500 hPa Difference ERA40-NCEP Variance HF: 1979-2002

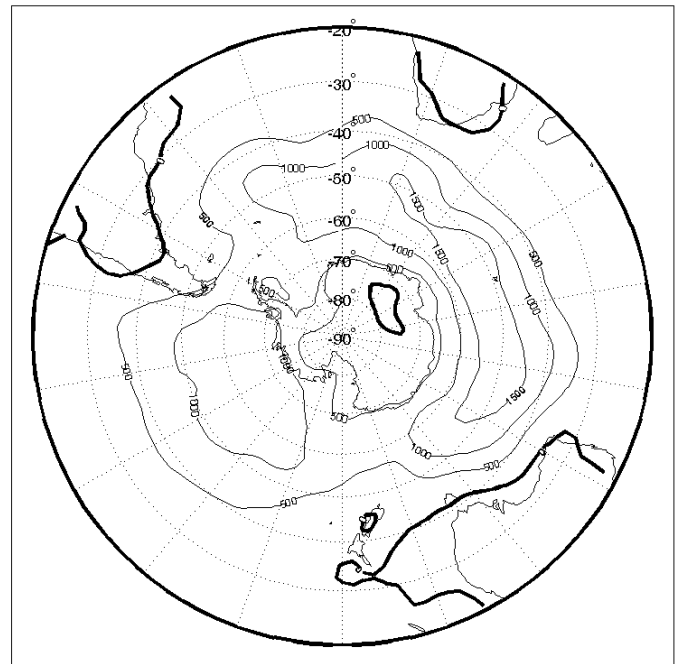


Figure 7: High frequency variance of the 500 hPa geopotential height, DJF period: a) NCEP 1958-1972; b) NCEP 1979-2002; c) difference between ERA40 and NCEP, 1958-72; d) as c) for 1979-2002. Units are m^2 and contour interval is $1000 m^2$ for a) and b) and $500 m^2$ for c) and d). Dashed lines pertain to negative values. Thick line corresponds to zero difference.

TABLES

$\Omega=\text{ALL}$	ERA 1957-2002	NCEP 1957-2002	ERA 40 1957-72	NCEP 1957-72	ERA 40 1979-2002	NCEP 1979-2002
$\bar{E}_T(\Omega)$	5100 \pm 100	4690 \pm 70	4610 \pm 90	4480 \pm 90	5600 \pm 100	4900 \pm 100
$\bar{E}_S(\Omega)$	1350 \pm 50	1270 \pm 40	1250 \pm 40	1240 \pm 50	1430 \pm 70	1230 \pm 70
$\bar{E}_E(\Omega)$	3740 \pm 70	3360 \pm 60	3430 \pm 80	3220 \pm 70	4040 \pm 90	3490 \pm 80
$\bar{E}_W(\Omega)$	1360 \pm 40	1330 \pm 40	1180 \pm 50	1260 \pm 50	1520 \pm 70	1340 \pm 60

Table 1: Time mean of $E_j(\Omega)$ with $j=T, S, E, W$ for the JJA period of the whole record, 1957-1972 and 1979-2002, respectively. We consider the standard error of the time-averaged value as a function of the interannual variability of the signal:

$$\Delta_{E_j(\Omega)} = \frac{\sigma_{E_j(\Omega)}}{\sqrt{N}}. \text{ As in Fig.3, } \Omega \text{ corresponds to the whole wave number and}$$

frequency domain. The units are m^2

Spectral properties	$k_1 = 2, k_2 = 4$	$k_1 = 5, k_2 = 72$
$\omega_1 = (2\pi/45)d^{-1}, \omega_2 = (2\pi/11)d^{-1}$	$\Omega = \text{LFLW}$	$\Omega = \text{LFHW}$
$\omega_1 = (2\pi/10)d^{-1}, \omega_2 = (2\pi/2)d^{-1}$	$\Omega = \text{HFLW}$	$\Omega = \text{HFHW}$

Table 2: Definition of 4 regions in the Hayashi spectra of the winter atmospheric variability; the symbol d is used as shorthand for ‘day’. *LFLW*: Low Frequency Long Wavenumber; *HFLW*: High Frequency Long Wavenumber; *LFHW*: Low Frequency High Wavenumber; *HFHW*: High Frequency High Wavenumber. Low

Frequency relates to periods from 11 to 45 days; High Frequency relates to periods from 2 to 10 days; Low Wavenumber relates to length scales larger than 1000Km; High wavenumber relates to length scales ranging from a few tens to hundreds of kilometres. The values $\omega_2 = (2\pi/2)d^{-1}, k_2 = 72$ constitute the highest frequency and wavenumber allowed by the adopted data resolution.

References

- Bengtsson, L., S. Hagemann, and K. I. Hodges, 2004: Can climate trends be calculated from reanalysis data?, *J. Geophys. Res.*, **109**, D11111, doi:10.1029/2004JD004536.
- Brankovic, C. and Molteni, F. 2004: Seasonal climate and variability of the ECMWF ERA-40 model, *Climate Dyn.*, **22**, 139–155.
- Cai, M. and Mak, M. 1990: Symbiotic relation between planetary and synoptic scale waves. *J. Atmos. Sci.* **47** 2953-2968.
- Dell'Aquila, A., Lucarini, V., Ruti, P.M., and S. Calmanti, 2005 . Hayashi Spectra of the Northern Hemisphere Mid-latitude Atmospheric Variability in the NCEP-NCAR and ECMWF Reanalyses. *Climate Dynamics, in press*.
- Fraedrich K, Bottger H (1978) A wavenumber frequency analysis of the 500 mb geopotential at 50°N. *J Atmos Sci* 35: 745-750
- Fraedrich, K. and E. Kietzig, 1983. Statistical analysis and wavenumber frequency spectra of the 500 mb geopotential along 50°S. *J. Atmos. Sci.* **40**, 1037-1045.
- Hansen, A.R., Sutra, A. and D.E. Venne, 1989 : An examination of midlatitude power spectra : evidence for standing variance and the signature of El Nino. *Tellus*, **41A**, 371-384.
- Hayashi. Y. 1971. A generalized method for resolving disturbances into progressive and retrogressive waves by space Fourier and time cross-spectral analysis. *J. Meteorol. Soc. Jap.*, **49**, 125-128.
- Hayashi Y. 1979: A generalized method for resolving transient disturbances into standing and travelling waves by space-time spectral analysis. *J. Atmos. Sci.*, **36**, 1017-1029.
- Kanamitsu M., Ebisuzaki E., Woollen J. , Shi-Keng Yang, J. J. Hnilo, M. Fiorino, and G. L. Potter, 2002: NCEP–DOE AMIP-II Reanalysis (R-2). *Bull. Am. Meteor. Soc.*, **83**, 1631-1643.
- Kalnay, E., Kanamitsu M, Kistler R, Collins W, Deaven D, Gandin L, Iredell M, Saha S, White G, Woollen J, Zhu Y, Leetmaa A, Reynolds R, Chelliah M, Ebisuzaki W, Higgins W, Janowiak J, Mo KC, Ropelewski C, Wang J, Jenne R, Joseph D. 1996. The NCEP/NCAR 40-Year Reanalysis Project. *Bull. Am. Meteor. Soc.*, **77**, 437–471.
- Kidson, J W, 1999: Principal modes of southern hemisphere low-frequency variability obtained from NCEP-NCAR reanalysis. *J. Climate*, **12**, 2808-2830.
- Kistler R, Kalnay E, Collins W, Saha S, White G, Woollen J, Chelliah M, Ebisuzaki W, Kanamitsu M, Kousky V, van den Dool H, Jenne R, Fiorino M,

- 2001: The NCEP-NCAR 50-year reanalysis: Monthly means CD-ROM and documentation. *Bull. Am. Meteorol. Soc.* **82**, 247–267
- Mechoso, C.R., and D.L. Hartmann, 1982: An observational study of travelling planetary waves in the Southern Hemisphere. *J. Atmos. Sci.* **39**, 1921-1935,
- Renwick, J.A. and M. J. Revell, 1999: Blocking over the South Pacific and Rossby Wave propagation. *Mon. Wea. Rev.* **127**, 2234-2247.
- Pratt RW (1976) The interpretation of space-time spectral quantities. *J Atmos Sci* 33: 1060–1066
- Santer, B. D., Sausen, R., Wigley, T. M. L., Boyle, J. S., AchutaRao, K., Doutriaux, C., Hansen, J. E., Meehl, G. A., Roeckner, E., Ruedy, R., Schmidt, G., and Taylor, K. E. 2003. Behavior of tropopause height and atmospheric temperature in models, reanalyses, and observations: Decadal changes. *J. Geophys. Res. (D1)* **108**, 1-22.
- Simmonds, I. and K. Keay, 2000: Mean Southern Hemisphere extratropical cyclone behavior in the 40-year NCEP–NCAR reanalysis. *J. Climate*, **13**, 550-561
- Simmons, A. J. and J. K. Gibson, 2000: The ERA-40 Project Plan, *ERA-40 Project Report Series No. 1*, ECMWF, 62 pp.
- Sterl A., 2004: On the (in-)homogeneity of reanalysis products, *J. Climate.*, **17**, 3866-3873
- Sturaro, G., 2003: A closer look at the climatological discontinuities present in the NCEP/NCAR reanalysis temperature due to the introduction of satellite data. *Climate Dyn.*, **21**, doi:10.1007/s00382-003-0348-y.
- Tibaldi, S., E. Tosi, A. Navarra, and L. Peduli, 1994: Northern and Southern Hemisphere seasonal variability of blocking frequency and predictability. *Mon. Wea. Rev.* **122**, 1971-2003.
- Trenberth, K E, 1991: Storm track in the southern hemisphere. *J. Atmos. Sci.* **48**, 2159-2178.